








Article

Efficient Arsenate Decontamination from Water Using MgO-Itsit Biochar Composite: An Equilibrium, Kinetics and Thermodynamic Study

Salah Ud Din ^{1,*}, Babar Hussain ¹, Sirajul Haq ^{1,*} , Muhammad Imran ² , Pervaiz Ahmad ³ ,
Mayeen Uddin Khandaker ⁴ , Fazal Ur Rehman ¹, Sayed M. Eldin ⁵ , Abd Allah A. Mousa ^{6,7} ,
Ilyas Khan ⁸ and Talha Bin Emran ^{9,10} 

¹ Department of Chemistry, University of Azad Jammu and Kashmir, Muzaffarabad 13100, Pakistan

² Department of Environmental Sciences, COMSATS University Islamabad, Vehari Campus, Vehari 61100, Pakistan

³ Department of Physics, University of Azad Jammu and Kashmir, Muzaffarabad 13100, Pakistan

⁴ Center for Applied Physics and Radiation Technologies, School of Engineering and Technology, Sunway University, Bandar Sunway 47500, Selangor, Malaysia

⁵ Center of Research, Faculty of Engineering, Future University in Egypt, New Cairo 11835, Egypt

⁶ Department of Mathematics and Statistics, College of Science, Taif University, Taif 21944, Saudi Arabia

⁷ Department of Basic Engineering Science, Faculty of Engineering, Menofia University, Shebin El-Kom 32511, Egypt

⁸ Department of Mathematics, College of Science Al-Zulfi, Majmaah University, Al-Majmaah 11952, Saudi Arabia

⁹ Department of Pharmacy, BGC Trust University Bangladesh, Chittagong 4381, Bangladesh

¹⁰ Department of Pharmacy, Faculty of Allied Health Sciences, Daffodil International University, Dhaka 1207, Bangladesh

* Correspondence: salah_mahsud@yahoo.com (S.U.D.); cii_raj@yahoo.com (S.H.)



Citation: Din, S.U.; Hussain, B.; Haq, S.; Imran, M.; Ahmad, P.; Khandaker, M.U.; Rehman, F.U.; Eldin, S.M.; Mousa, A.A.A.; Khan, I.; et al.

Efficient Arsenate Decontamination from Water Using MgO-Itsit Biochar Composite: An Equilibrium, Kinetics and Thermodynamic Study. *Water* **2022**, *14*, 3559. <https://doi.org/10.3390/w14213559>

Academic Editors: Changseok Han, Daphne Hermosilla Redondo, Yejoon Yoon and Alicia L. Garcia-Costa

Received: 20 September 2022

Accepted: 31 October 2022

Published: 5 November 2022

Publisher's Note: MDPI stays neutral with regard to jurisdictional claims in published maps and institutional affiliations.



Copyright: © 2022 by the authors. Licensee MDPI, Basel, Switzerland. This article is an open access article distributed under the terms and conditions of the Creative Commons Attribution (CC BY) license (<https://creativecommons.org/licenses/by/4.0/>).

Abstract: (1) Background: In this investigation, a composite of MgO nanoparticles with Itsit biochar (MgO-IBC) has been used to remove arsenate from contaminated water. The reduced adsorption capacity of biochar (IBC), due to loss of functionalities under pyrolysis, is compensated for with the composite MgO-IBC. (2) Methods: Batch scale adsorption experiments were conducted by using MgO-IBC as an adsorbent for the decontamination of arsenate from water. Functional groups, elemental composition, surface morphology, and crystallinity of the adsorbent were investigated by using FTIR, EDX, SEM and XRD techniques. The effect of pH on arsenate adsorption by MgO-IBC was evaluated in the pH range of 2 to 8, whereas the temperature effect was investigated in the range of 303 K to 323 K. (3) Results: Both pH and temperature were found to significantly influence the overall adsorption efficiency of MgO-IBC for arsenate adsorption with lower pH and higher temperature being suitable for higher arsenate adsorption. A kinetics study of arsenate adsorption confirmed an equilibrium time of 240 min and a pseudo-second-order model well-explained the kinetic adsorption data, whereas the Langmuir model best fitted with the equilibrium arsenate adsorption data. The spontaneity and the chemisorptive nature of arsenate adsorption was confirmed by enthalpy, entropy, and activation energy. Comparison of adsorbents in the literature with the current study indicates that MgO-IBC composite has better adsorption capacity for arsenate adsorption than several previously explored adsorbents. (4) Conclusions: The higher adsorption capacity of MgO-IBC confirms its suitability and efficient utilization for the removal of arsenate from water.

Keywords: Itsit biochar; adsorption; arsenic; composites

1. Introduction

Arsenic is a poisonous and harmful chemical present in the Earth. It is a slow poisonous chemical that has a negative impact on human health. Arsenic is found naturally

in minerals and rocks. Arsenic encounters ground water due to erosion and weathering of earth materials as well as volcanic emissions and causes contamination of the water resources. In contrast with natural sources, man-made activities such as mining, industrial chemical waste, fossil fuel combustion and arsenic pesticides contribute to arsenic contamination [1]. It has been utilized in paints, pigmenting substances, and dyes and is primarily employed as a wood preservative in industry. Also, it is used in the glass and electronics sectors, as well as in the tanning of leather [2]. Arsenic is utilized in tiny amounts in the medication of living organisms and in care items and is found in many dietary supplements [3]. As a result, the use of arsenic-containing compounds causes hyperkeratosis, conjunctivitis, hyperpigmentation, peripheral vascular system and central nervous system disorders, limb gangrene, skin cancer and cardiovascular diseases [4]. Therefore, arsenic-contaminated water must be treated before ingestion.

Different countries, including India, China [5], Vietnam, Taiwan, United States, Chile [6,7], Argentina, Mexico [8], Bangladesh [9], Poland, New Zealand, Japan, Canada and Hungary [10] are badly affected by arsenic-contaminated water. West Bengal (India) and Bangladesh are two of the most arsenic-polluted countries in the world, with arsenic levels in drinking water well above the WHO standard of $10 \mu\text{g L}^{-1}$ [11]. Arsenic occurs in a variety of oxidation states in nature. It can arise in both organic and inorganic forms in water. Arsenic in its inorganic forms, such as As (III) and As (V) is very hazardous to humans and is not removed by simple treatment methods. A number of methods, such as membrane filtration, reverse osmosis and ion exchange [12], precipitation and oxidation [13], adsorption [14], nanofiltration [15] and coagulation–flocculation [16], have been employed for arsenic mitigation. Each of these techniques has its own set of advantages and drawbacks, making it difficult to choose the best one. Traditional methods have several drawbacks, including high sludge generation, membrane fouling, high cost and, in the case of ion exchange, constant ions concentration monitoring [17]. With all the disadvantages of the above-mentioned techniques to be considered, adsorption is concluded to be the best among these common methods for removing arsenic from aqueous solutions, and it is now regarded as an efficient and cost-effective method of water treatment [18,19].

There are many adsorbents which have been used for the decontamination of arsenate from water, including oxides/hydroxides of iron, activated carbon, zinc oxide and many biosorbents [20–22]. Popular among these adsorbents and widely considered as being suitable due to their high surface area and adsorption capacity are magnesium oxide and activated alumina P [23,24]. However, application of activated alumina for arsenate decontamination is restricted due to the hazardous nature of aluminum. In contrast, nanoparticles of magnesium oxide are better for arsenate detoxification due to greater interaction between arsenate ions and magnesium ions [25]. However, the metallic nanoparticles often exhibit the problem of particle aggregation during adsorption, which is complicated for adsorption studies. To get rid of this difficulty, nanocomposites with carbon rich materials, e.g., biochar, are considered a better option for the decontamination of several contaminants from water. Hence, biochar with high porosity is found to be efficient as a carrier for magnesium nanoparticles and is very cost effective compared to the popular activated carbon. Biochar alone, however, cannot offer the desired adsorption potential for arsenate due to loss of functionalities owing to heat treatment which results in a decrease in adsorption sites [26].

The current investigation deals with studying the potential of the Itsit plant for synthesizing its biochar and its nanocomposite with magnesium oxide nanoparticles for the decontamination of arsenate from water. The MgO nanoparticles play a significant role in enhancing the sorption capacities of biochar by improving surface characteristics (functional groups and adsorption sites) with greater interaction for arsenate on the surface of the biochar [27,28]. Batch scale adsorption experiments were used in this study to test the potential of arsenate adsorption on the surface of a composite of magnesium oxide with Itsit biochar (MgO-IBC).

2. Materials and Methods

2.1. Synthesis of Itsit Biochar (IBC)

To prepare Itsit biochar (IBC), *Trianthema portulacastrum* (Itsit) biomass (TPB) was first collected from the field, washed with distilled water, and then air dried. Subsequently, TPB was cut into small pieces (1–1.5 cm) and biochar of TPB, also known as Itsit biochar (IBC), was prepared at 400 °C at 8–10 °C/min. During biochar preparation, nitrogen was injected at a rate of 50 cm³/min.

2.2. Synthesis of IBC Composite with Magnesium Oxide Nanoparticles

To prepare the composite of IBC with magnesium oxide nanoparticles (MgO-IBC), magnesium chloride (MgCl₂) salt and potassium hydroxide (KOH) were used. A 0.1 M solution (1 L) of MgCl₂ and 0.12 M KOH solution (1 L) were prepared in distilled water. The solution of MgCl₂ (100 mL) and 0.5 g of IBC was thoroughly mixed for 10 min. Subsequently, this mixture was titrated with KOH (100 mL), dropwise, to prepare the MgO-IBC nanocomposite. The resultant MgO-IBC nanocomposite was filtered and dried in an oven at 90 °C for 36 h.

2.3. Characterization of Materials

A Fourier-transform infrared (FTIR) spectrometer (Alpha, Bruker, Germany) was run in the range of 4000–400 cm⁻¹ using KBr pellets to identify the functional groups of the biochar composite. Scanning electron microscopy (SEM) (NOVA FEISEM 450, Tokyo, Japan) was used to analyze the morphological aspects of MgO-IBC. While the elemental composition of biochar composite was determined with an energy dispersive X-ray spectrophotometer (EDX 2800B ROHS analyzer X, Oxford instruments, Oxfordshire, UK). The point of zero charge (PZC) was determined to evaluate the overall surface charge of the adsorbent's surface using a KCl electrolyte solution [18,19]. For PZC determination, 40 mL of 0.1 M KCl solution was taken in various flasks. The initial pH of these solutions was adjusted (2–8) and 0.1 g of MgO-IBC was added into each flask. The flasks were shaken in a shaker bath, at a temperature of 298 K, for 24 h. After an equilibrium time, the final pH was noted after 24 h; change in pH (Δ pH) was plotted with initial pH and the point crossing the zero of Δ pH was taken as the PZC. Moreover, the crystallinity in the biochar and its composite was analyzed with an X-ray diffractometer (XRD) (Malvern Pananalytical, Malvern, UK) having a current voltage of 40 mA and a radiation source of Cu at 45 kV. The Scherrer equation [18] was used to calculate the crystallite size from the XRD data of MgO-IBC.

2.4. Adsorption Studies of Arsenic onto MgO-IBC

A batch study was conducted to examine the performance of the MgO-IBC nanocomposite at varying temperatures, arsenic concentrations, and solution pH. The influence of pH on arsenic adsorption was studied by adding 0.05 g MgO-IBC nanocomposite to 40 mL of arsenate solution (500 μ g L⁻¹) at 298 K and by adjusting the pH from 2–8 with the help of 0.1 M HNO₃ and 0.1 M NaOH. The influence of temperature was evaluated by taking 0.05 g of adsorbent in 30 mL of arsenate solutions of various concentrations (20 to 500 μ g L⁻¹) while maintaining the pH at 5 in the temperature range of 303 to 323 K. The arsenic containing flasks, after shaking in a shaker bath, were finally filtered and analyzed for remaining arsenic concentration using an atomic absorption spectrophotometer.

The kinetic effect of arsenate adsorption by MgO-IBC nanocomposite was investigated by taking 40 mL of 500 μ g L⁻¹ arsenate solution with a 0.1 g dose of MgO-IBC nanocomposite. These flasks were shaken well in a shaker bath from 5 min to 24 h at 298, 308 and 313 K and at pH 5. The samples were collected at different times and were analyzed for remaining arsenic concentration in water after the interaction with MgO-IBC.

2.5. Reusability and Stability Study of MgO-IBC

Thirty mL of arsenate solution ($500 \mu\text{g L}^{-1}$) was taken in a flask and 0.05 g MgO-IBC composite was added to it at pH 5. This suspension was shaken well for 3 h and then filtered to determine the residual arsenic concentration in water. This arsenic-loaded adsorbent was rinsed with 30 mL of 6% HCl solution, for desorption of arsenic, and then was oven-dried. The dried MgO-IBC, after rinsing with acid solution, was again used for arsenic adsorption and this process of desorption/adsorption was repeated in four cycles. Magnesium concentration was measured in the acidic solution after each rinsing to evaluate the stability of MgO-IBC.

3. Results

3.1. FTIR Analysis

FTIR patterns of Itsit biochar (IBC) and its composite with MgO (MgO-IBC) are shown in Figure 1a,b, respectively. The broad band around $3400\text{--}3600 \text{ cm}^{-1}$ indicates the OH vibrational stretch of the hydroxyl phenolic functional group containing hydrogen bonding due to adsorption of water molecules. Similarly, the peaks around 1611 cm^{-1} and 1396 cm^{-1} can be attributed to the secondary amine and bending vibration of O–H or C–O phenolic vibrational stretch, respectively [29], while a small band in the range of $1124\text{--}1274 \text{ cm}^{-1}$ indicates the existence of C–H bending due to the presence of alkanes or an alkyl group [30]. The small band at 614 cm^{-1} is due to C–H vibrational stretch. Some extra peaks are observed in the composite biochar in Figure 1b. The peaks observed at 1715 cm^{-1} can be assigned to C=C, whereas the peak at 1633 cm^{-1} indicates C=O vibrational stretch of the carboxylic group. The band in the range of $1367\text{--}1228 \text{ cm}^{-1}$ is attributed to C–O–C symmetric stretch whereas the peak at 1101 cm^{-1} shows the presence of alcohol. The small peaks around 538 cm^{-1} confirmed the Mg–O vibration [31].

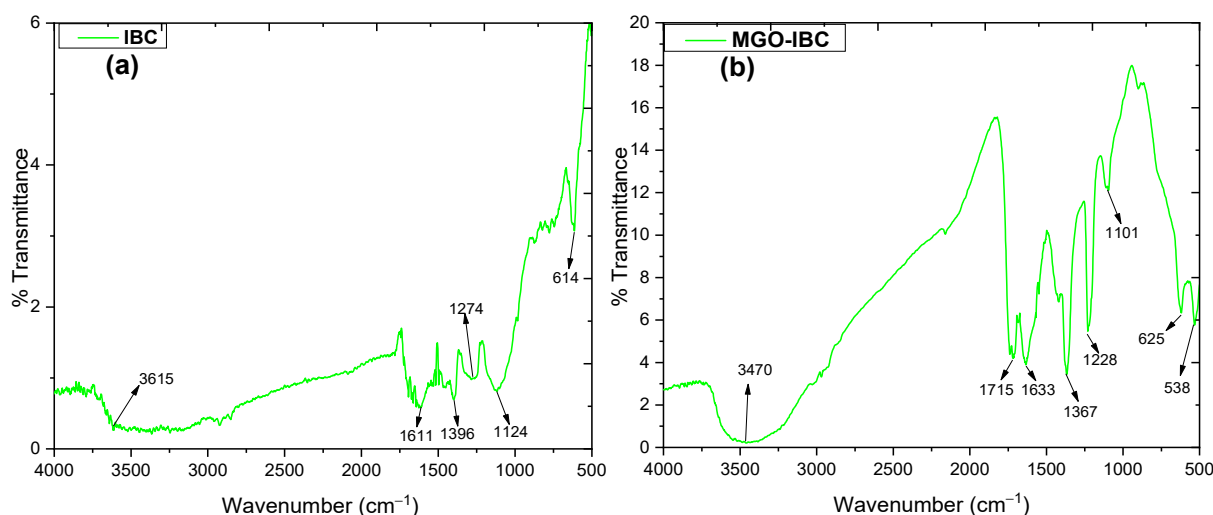


Figure 1. FTIR spectra of (a) IBC (b) MgO-IBC composite.

3.2. XRD Analysis

The XRD results (Figure 2a) of IBC identified the amorphous nature of the biochar sample, whereas MgO-IBC crystallinity was observed in the structure of biochar as confirmed by the appearance of peaks in Figure 2b. These peaks in the composite of biochar appeared at 2θ values of 50.8° and 58.6° , having miller indices (110) and (111), respectively, which indicates the hexagonal crystalline planes of $\text{Mg}(\text{OH})_2$ [32]. Moreover, peaks at $2\theta = 37.2^\circ$, 43.3° , 62.5° and 79.3° , with miller indices (111), (200), (220) and (222), show the appearance of MgO nanoparticles with cubic polycrystalline structure (JCPDS No. 87-0653). The crystallite size of MgO-IBC composite was 14.7 nm indicating the particle size in the nano-range.

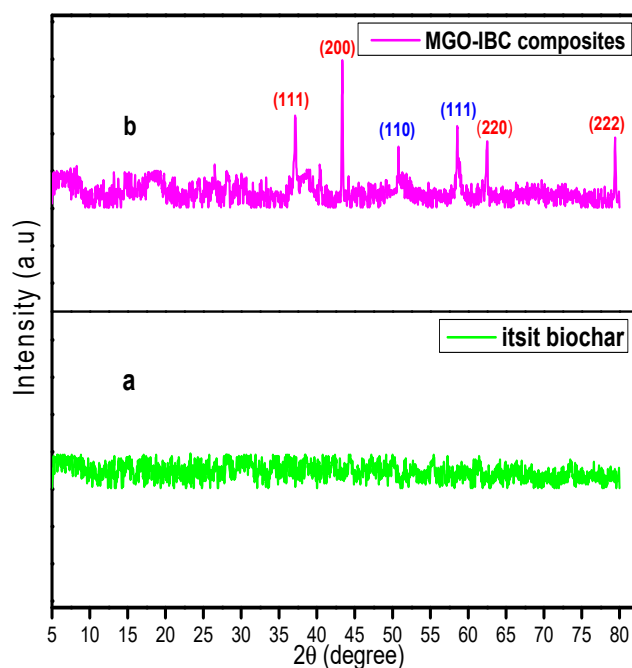


Figure 2. XRD spectrum of (a) IBC and (b) MgO-IBC composite.

3.3. SEM Analysis

The surface morphology of IBC and MgO-IBC was investigated with scanning electron microscopy (SEM) as shown in Figure 3a–d. SEM images of IBC (Figure 3a,b) show irregularities in size. However, the micrographs of MgO-IBC (Figure 3c,d) clearly show the deposition of MgO on the biochar surface. Owing to the presence of the small-sized MgO nanoparticles, the surface roughness of the IBC increases, which is suitable for heavy metal adsorption [33,34].

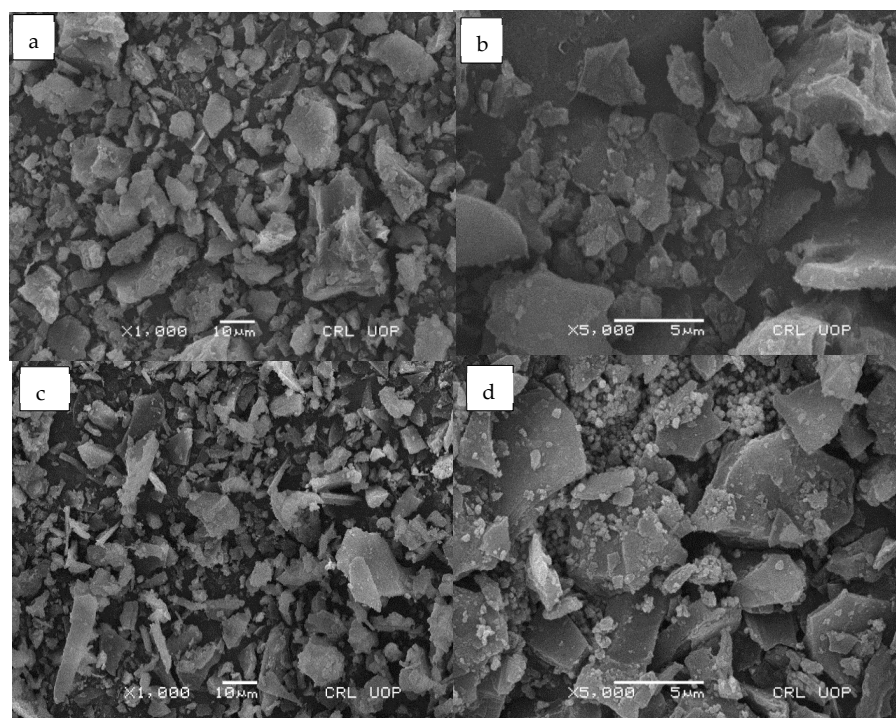


Figure 3. SEM micrograph of IBC at the magnification of (a) 10 μm (b) 5 μm and MgO-IBC composite at (c) 10 μm (d) 5 μm.

3.4. EDX Analysis

EDX analysis of IBC and MgO-IBC was conducted to determine the elemental composition of the samples as shown in Figure 4a,b. The EDX indicates a high content of carbon (62.46%) and oxygen (15.39%) and low contents of Na, Mg, Al, Si, P, S, Cl, K, Ca and Cu in the IBC biochar. However, the percentage of O was found to increase to 27.19% in the composite biochar as compared to the IBC (15.39%) in addition to the presence of Mg (14.04%), which confirms the successful impregnation of MgO in the biochar composite [26].

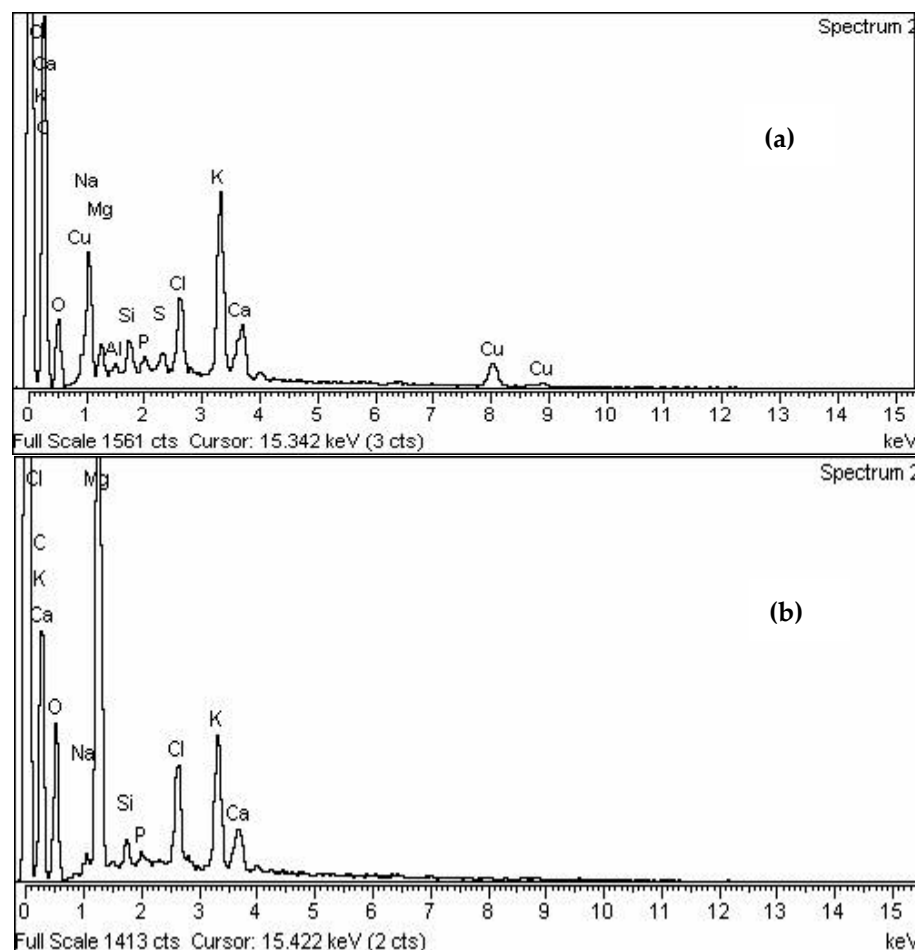


Figure 4. (a) EDX spectrum of IBC, (b) EDX spectrum of MgO-IBC composite.

3.5. Point of Zero Charge (PZC)

The point of zero charge is the pH at which the adsorbent surface has a net zero charge and is calculated by plotting Δ pH vs pH and the intersection point of the curve at zero is taken as the PZC. The PZC of MgO-IBC composite in the present investigation was pH 6.6 (Figure 5).

3.6. Effect of Contact Time

The effect of contact time on arsenic adsorption by MgO-IBC composite was studied at times varying from 5 to 420 min, pH 5 and a temperature range of 303 K to 323 K, as shown in Figure 6. It can be observed from the results that initially, with the increase in contact time, the arsenate sorption rate increased quickly, which resulted in greater removal of arsenate by MgO-IBC due to availability of more active sites. As the equilibrium time approached 300 min, efficiency of removal started to decrease gradually until 420 min, after which no rise in adsorption rate was observed, which is attributed to the saturation of all active sites. The influence of temperature on the kinetics of arsenate adsorption by MgO-

IBC was lower in the first 20 min, after which the sorption process increased significantly with the increase in temperature. Initially, the arsenate ions at all the temperatures had the availability of enough adsorption sites on the surface of the adsorbent. However, with the saturation of adsorbent’s surface, only an increase in temperature created additional surface sites on the surface of the adsorbent due to bond breakage of Mg-O on the surface of composite. Moreover, an increase in temperature also led to increased movement of arsenate ions towards the adsorbent’s surface leading to enhanced adsorption. However, there was no significant effect of temperature observed at the equilibrium time of this investigation. A similar trend of initial rise and subsequent fall in adsorption has also been reported elsewhere [18,35].

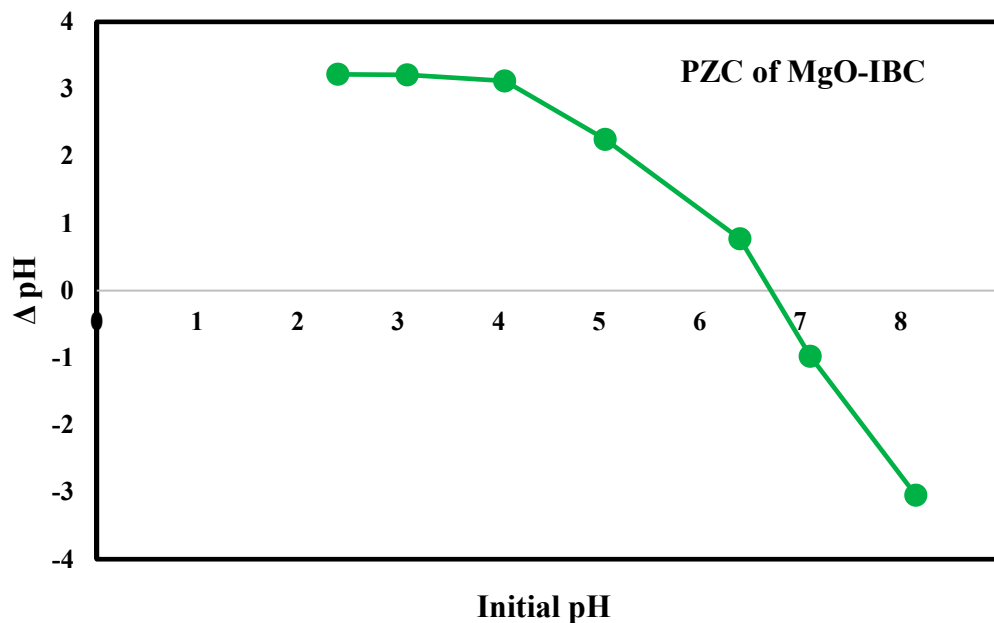


Figure 5. Point of zero charge of MgO-IBC composite.

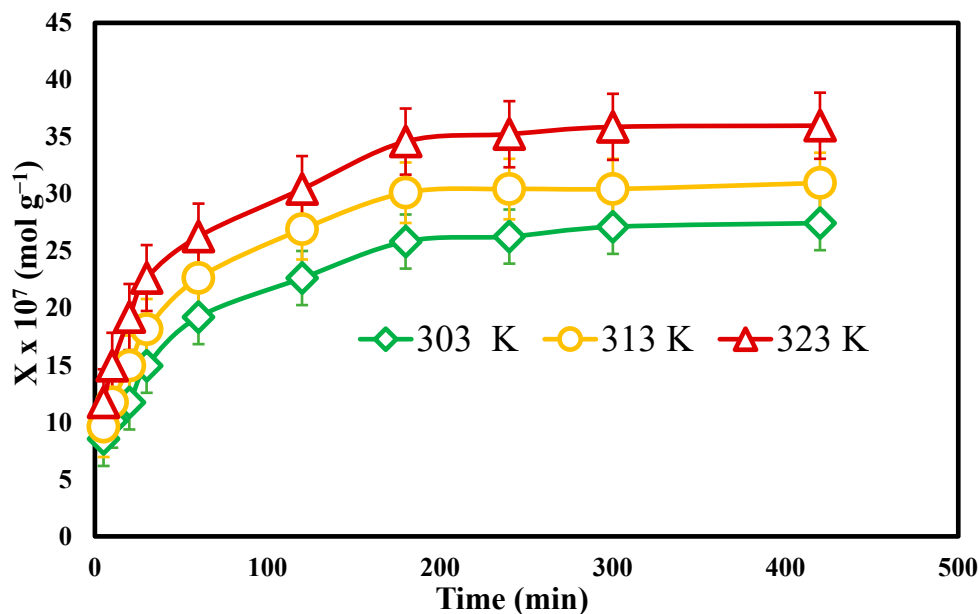


Figure 6. Effect of contact time on arsenate adsorption on to MgO-IBC composite at pH 5.

3.7. Effect of pH

Changing the pH of the solution has a significant effect on arsenic adsorption by the adsorbent and this effect was studied in the pH range of 2 to 8 and at a temperature of 298 K, as shown in Figure 7. It can be observed that, at lower pH values maximum adsorption was observed due to development of attractive forces between the negative arsenate ions ($\text{H}_2\text{AsO}_4^{-1}$ and HAsO_4^{-2}) and the positive adsorbent surface and $\text{pH} < \text{PZC}$ (6.6). The lower the pH, the more negatively charged arsenic ions are adsorbed resulting in higher arsenic adsorption at low pH. When pH increases, the repulsive forces are generated between the post PZC negative adsorbent's surface and the negative arsenate ions, which decreases the extent of adsorption at higher pH values [36]. Moreover, at higher pH values, an increase in negative OH ions also offers competition to the negative arsenate anions, leading to a decrease in the adsorption of arsenate at higher pH values. A similar trend of higher adsorption at lower pH and lower adsorption at higher pH values has been observed elsewhere [18,37].

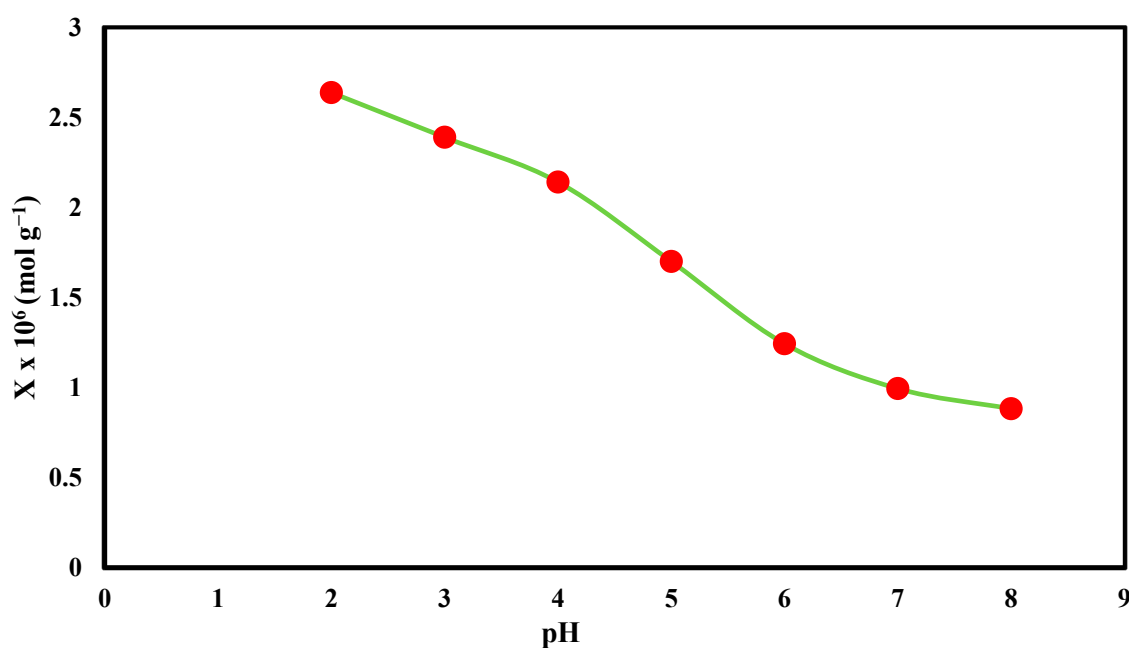


Figure 7. Effect of pH on arsenate adsorption onto MgO-IBC composite.

3.8. Effect of Temperature and Concentration

Both concentration and temperature are the forces that control the adsorption system. The effect of concentration and temperature was investigated in the present investigation at pH 5 in the concentration range of 20 to 500 $\mu\text{g L}^{-1}$ when the temperature was 303, 313 and 323 K (Figure 8). Results revealed that an increase in concentration and temperature was found to have a positive effect on arsenate adsorption on the surface of MgO-IBC. However, the adsorption slows down considerably after a certain increase in concentration leading to an equilibrium condition. This initial increase in adsorption was due to the availability of more adsorption sites which became limited as the concentration of arsenate ions increased leading to equilibrium conditions. At a higher temperature, more adsorption sites are created at the surface of the composite due to more bond breakage of Mg-O resulting in displacement of oxygen by arsenate ions and thereby increasing the adsorption at higher temperature [38,39]. Moreover, increased diffusion of arsenate ions within the adsorbent pore space is another factor leading to increased adsorption at higher temperatures [40].

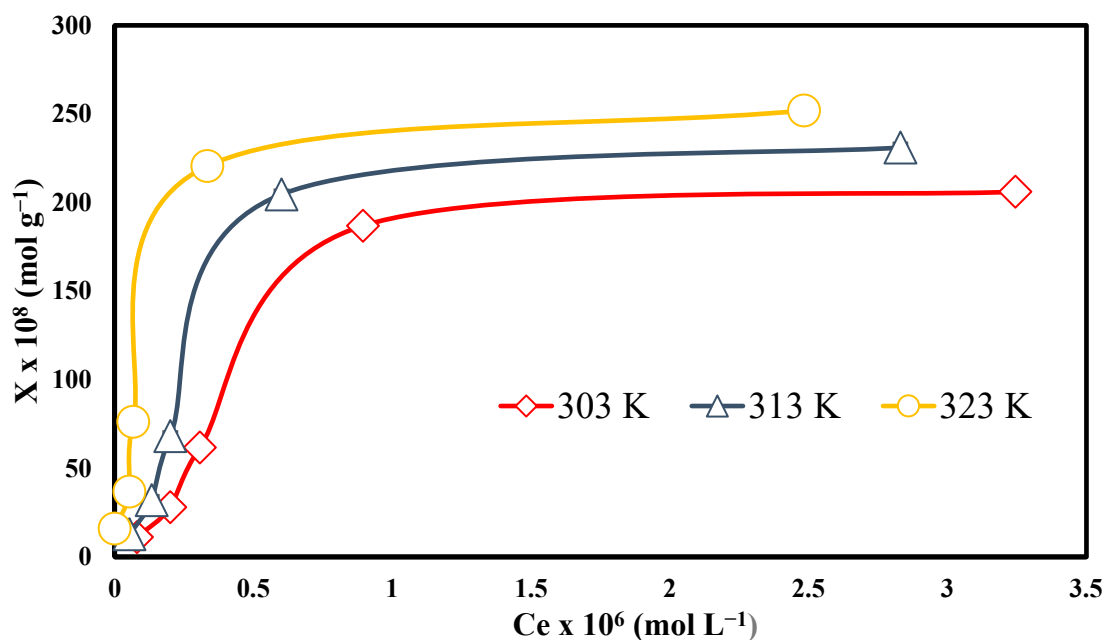


Figure 8. Effect of temperature and concentration on arsenate adsorption onto MgO-IBC composite at pH 5.

3.9. Ho and Mckay’s- Plot

To have an insight into the mechanism of arsenate adsorption by MgO-IBC, the kinetic data were subjected to the linearized form of Lagergren (pseudo first order) and Ho and Mckay’s (pseudo second order) models according to the Equations (1) and (2) respectively,

$$\log(X_e - X_t) = \log(X_e) - \frac{k_1}{2.303}t \tag{1}$$

$$\frac{t}{X_t} = \frac{1}{k_2 X_e^2} + \frac{t}{X_e} \tag{2}$$

where X_t and X_e (mol g^{-1}) in the above equations represent arsenic concentration adsorbed at time ‘t’ and at equilibrium, respectively, whereas k_1 and k_2 are pseudo-first-order and pseudo-second-order rate constants. Straight lines in both cases were obtained when graphs were plotted between time t and $\ln(X_e - X_t)$ (pseudo-first-order plot) and t/X_e vs. t (pseudo-second-order plot) as shown in Figure S1 and Figure 9 respectively. However, higher R^2 values are obtained with a pseudo-second-order plot which confirms a pseudo-second-order plot to be the model applicable to the kinetic data. The applicability of the pseudo-second-order model and an increase in the values of pseudo-second-order rate constants and X_e with the increase in the temperature of the system (Table 1) indicate the process of adsorption to be endothermic and chemisorptive in nature [37].

Table 1. Pseudo second order model parameters and activation energy for arsenate adsorption on MgO-IBC composite.

Temperature (K)	k_2 ($\text{g m}^{-1} \text{mol}^{-1}$)	$X_e \times 10^7$ (mol g^{-1})	E_a (kJ mol^{-1})
303	1.41	29.010	20.61
313	1.49	32.562	
323	1.57	37.707	

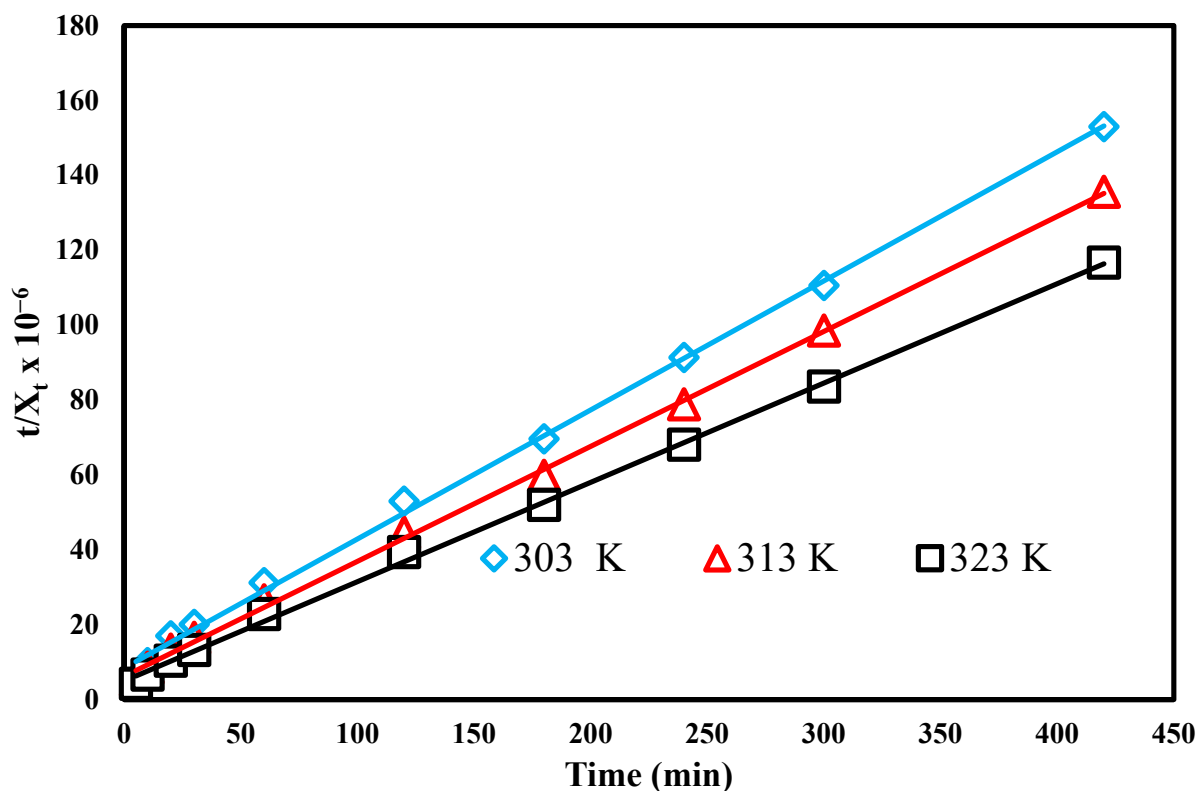


Figure 9. Correlation of pseudo-second-order kinetic model and experimental adsorption of arsenate on MgO-IBC composite.

3.10. Langmuir Model

The Langmuir model assumes adsorption to be monolayer in nature. The Langmuir model in its linearized form (Equation (3)) was used for arsenate adsorption on the surface of MgO-IBC composite.

$$\frac{C_e}{X} = \frac{1}{X_{\max} \times K_b} + \frac{C_e}{X_{\max}} \quad (3)$$

where C_e (mol L^{-1}) is the concentration of arsenate at equilibrium and X (mol g^{-1}) represents adsorption of arsenate ions (mol g^{-1}). A plot between C_e/X vs. C_e , as shown in Figure 10, indicates a well-fitted linear plot with a correlation coefficient greater than 0.99, which shows the applicability of the Langmuir model confirming adsorption to be monolayer in nature. Furthermore, an increase in temperature resulted in the increase in the adsorption capacities (X_m) confirming the adsorption process to be endothermic in nature [13]. The increase in the values of K_b with temperature indicates that strong binding forces are involved in the adsorption process (Table 2). The comparison of the calculated values of X_m in the present investigation with the literature (Table 3) shows the adsorption capacity of MgO-IBC for arsenic to be greater than various adsorbents reported in the literature indicating it to be a very effective adsorbent for arsenic removal.

Table 2. Parameters of the Langmuir model for arsenate adsorption on MgO-IBC composite.

Temperature (K)	$X_{\max} \times 10^2$ (mg g^{-1})	$K_b \times 10^{-4}$ (L mol^{-1})
303	19.7	2.018
313	23.1	9.103
323	24.3	15.43

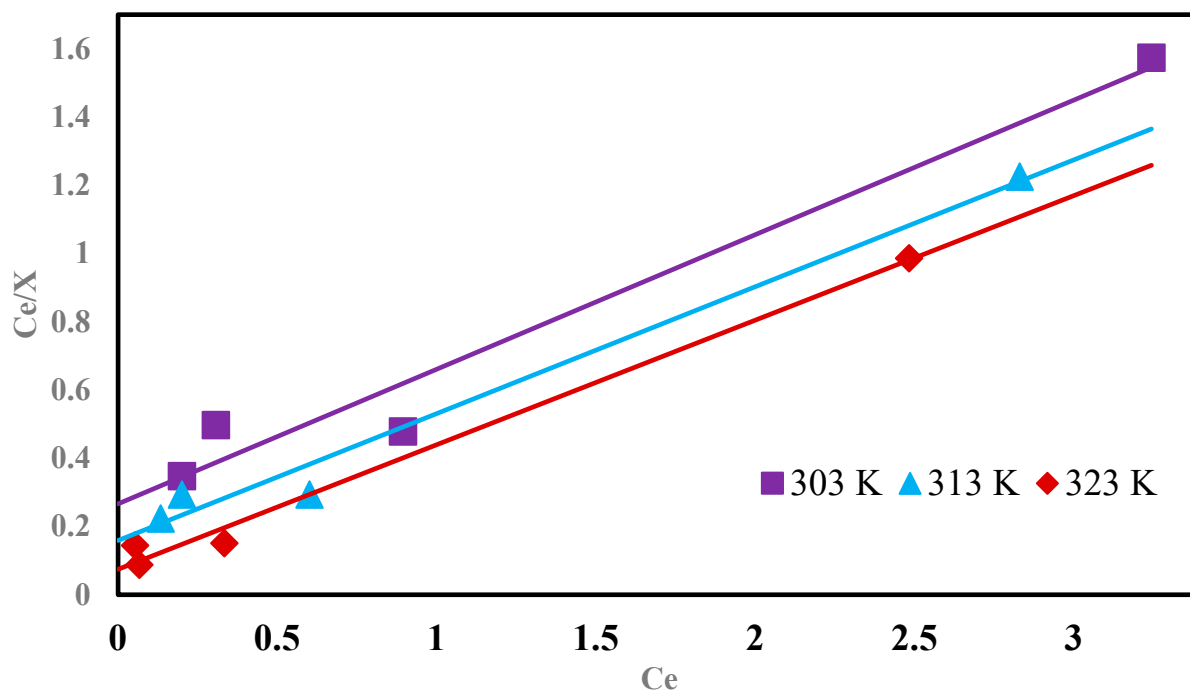


Figure 10. Langmuir plot of arsenate adsorption on MgO-IBC composite.

Table 3. Comparison of the adsorption capacities of different adsorbents for arsenic.

Adsorbent	X_m (mg g ⁻¹)	References
Zn-loaded biochar	0.28	[41]
Ferromanganese oxide–biochar	0.712	[42]
Lignocelluloic	0.94	[43]
Nano-zerovalent iron biochar	1.40	[44]
Integrated active biochar filter	2.12	[45]
Animal-derived biochar	2.76	[46]
Fe-Mn-La-impregnated biochar	3.18	[47]
Japanese-oak-wood biochar	3.89	[48]
Metal-modified biochar	4.12	[49]
FeCl ₃ -activated biochar	4.4	[50]
MgO-IBC composite	4.86	Current study

3.11. Estimation of Activation Energy

For the activation energy (E_a) calculation, the Arrhenius Equation (4) was applied to the data in the linearized form as follows:

$$\ln k_2 = \ln A - \frac{E_a}{RT} \quad (4)$$

where k_2 is the pseudo-second-order rate constant, T is temperature in Kelvin (K), A is the pre-exponential factor and R represents the general gas constant. Activation energy was determined from the intercept and slope of the plot between $\ln k_2$ vs. T^{-1} (Figure S2). The E_a value calculated from the plot has been shown in Table 1 which is in the range of 8.4–83.7 kJ mol⁻¹, confirming the adsorption process to be chemisorptive in nature [51]. However, the adsorption is diffusion controlled in this case as the activation energy is less than 42 kJ mol⁻¹, in contrast to a chemically controlled process having $E_a > 42$ kJ mol⁻¹ [52]. Chemical adsorption occurs at the adsorption sites, but before that arsenate ions need to be transported by diffusion to the adsorption sites for the occurrence of the chemical reaction between arsenate ions and the adsorption site. Diffusion, being the slowest step, controls the overall rate in the series of steps leading to chemical adsorption [53].

3.12. Thermodynamic Parameters

Equations (5) and (6) were employed for the determination of the thermodynamic behavior of arsenate adsorption on MgO-IBC.

$$\ln k_b = \frac{\Delta S}{R} - \frac{\Delta H}{RT} \quad (5)$$

$$\Delta G = \Delta H - T\Delta S \quad (6)$$

where T, R, ΔH , ΔS , k_b and ΔG are temperature in K, general gas constant, enthalpy, entropy, binding energy constant and free energy, respectively. k_b was calculated from the Langmuir adsorption plot. The intercept and slope obtained from the plot between $\ln k_b$ vs. T^{-1} (Figure S3) are used for the calculation of ΔS and ΔH . Adsorption of arsenate on the surface of MgO-IBC nanocomposite is an endothermic process as indicated by the positive value of enthalpy of activation (Table 4). This means that conversion of reactants into product requires more energy as arsenate ions need to displace water molecules to be adsorbed on the composite surface. Entropy in the present investigation is positive which shows the high randomness at the interface of solid and liquid due to structural changes in the solid-liquid system [20]. ΔG values in the current investigation are negative, indicating the process of adsorption to be spontaneous and becoming more feasible with the increase in temperature. Similar values of thermodynamic parameters are observed elsewhere [54,55].

Table 4. Thermodynamic parameters for arsenate adsorption on MgO-IBC composite.

ΔH (kJ mol ⁻¹)	ΔS (J mol ⁻¹)	ΔG (kJ mol ⁻¹) 303 K	ΔG (kJ mol ⁻¹) 313 K	ΔG (kJ mol ⁻¹) 318 K
83.28	0.3584	-24.97	-29.71	-32.08

3.13. Reusability and Stability Study of MgO-IBC

The reusability of the MgO-IBC composite was checked by adsorption/desorption cycles and the data are shown in Figure 11. The removal percentage of MgO-IBC composite decreases from cycle 1 to 4 as shown in Figure 11. In the first cycle, 95.85% of arsenic was removed and arsenate removal (%) dropped to 86.18, 64.49 and 31.86% respectively in second, third and fourth cycle. The arsenic-loaded adsorbent was washed with 6% HCl solution and recycled. Maximum arsenate removal occurred in the first cycle due to the presence of large active sites which reduced greatly in the next cycles [19]. In all four cycles, the concentration of magnesium leaching back to the solution was well below the standard permissible limit (50 mg L⁻¹) showing the stability of the adsorbent as well as the better impregnation of magnesium with the biochar. The result shows the valuable stability, regeneration capacity and environmentally friendly nature of the MgO-IBC.

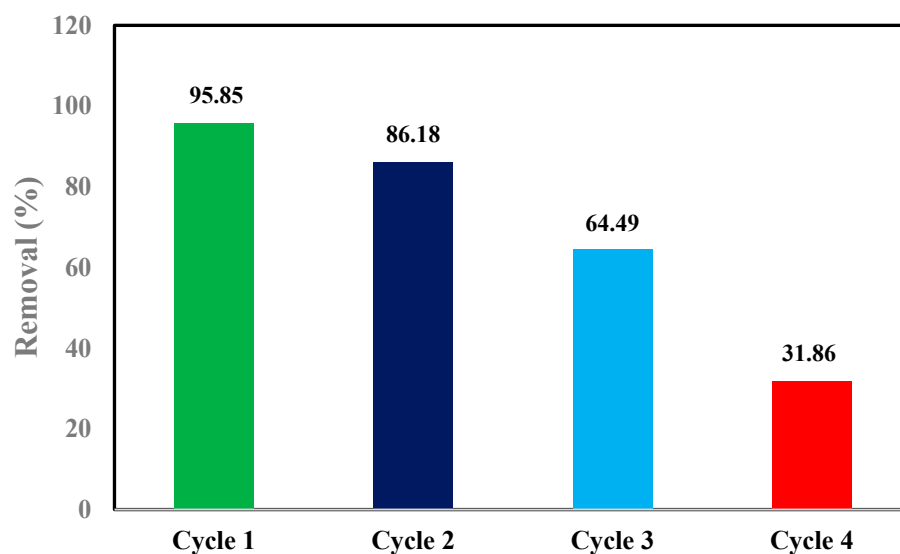


Figure 11. Reusability of MgO-IBC for the removal of arsenate in four adsorption/desorption cycles.

4. Conclusions

The current investigation explores the removal of arsenate by MgO-IBC composite. The FTIR spectrum of MgO-IBC shows extra peaks compared to raw biochar, confirming the formation of MgO bonding with the biochar, whereas SEM confirmed the increased roughness of the surface of the composite compared to raw biochar. The XRD analysis also further confirms composite formation due to the appearance of peaks of MgO. The Scherrer formula confirmed the crystallite size of the MgO-IBC composite as 14.7 nm. Lower pH and higher temperature were found to favorably enhance the adsorption of arsenate onto MgO-IBC. The kinetics study established 240 min as equilibrium time and the data were found to obey a pseudo-second-order model. Activation energy confirmed the chemical nature of the adsorption with a diffusion-controlled process. Monolayer coverage was confirmed by the applicability of the Langmuir model to the adsorption data. Thermodynamic parameters showed the process to be endothermic in nature. Higher adsorption capacity compared to various other adsorbents reported in the literature confirms the suitability and efficiency of MgO-IBC composite for the removal of arsenate by adsorption from water.

Supplementary Materials: The following supporting information can be downloaded at: <https://www.mdpi.com/article/10.3390/w14213559/s1>, Figure S1: Pseudo first order kinetics model of arsenate adsorption on MgO-IBC composites; Figure S2: Arrhenius plot of arsenate adsorption on MgO-IBC composites at pH 5; Figure S3: Vant Hoff's plot for arsenate adsorption on MgO-IBC composites.

Author Contributions: Conceptualization, S.U.D. and S.H.; methodology, T.B.E., S.H. and P.A.; software, S.M.E., A.A.A.M., M.U.K. and F.U.R.; validation, I.K., F.U.R. and T.B.E.; formal analysis, B.H. and P.A.; investigation, M.I.; resources, S.U.D., P.A. and S.H.; data curation, M.I.; writing—original draft preparation, B.H., A.A.A.M., M.U.K. and S.U.D.; writing—review and editing, A.A.A.M., T.B.E., S.M.E. and I.K.; visualization, M.U.K.; supervision, S.U.D.; project administration, S.H., S.U.D. and P.A.; funding acquisition, T.B.E., S.M.E., I.K. and A.A.A.M. All authors have read and agreed to the published version of the manuscript.

Funding: This research was funded by Higher Education Commission of Pakistan, grant number 8376.

Institutional Review Board Statement: Not applicable.

Informed Consent Statement: Not applicable.

Data Availability Statement: All the data is enclosed in the manuscript.

Acknowledgments: Salah Ud Din is thankful to the Higher Education Commission of Pakistan for research funding under the National research program for universities (NRPU) under project No. 8376.

Conflicts of Interest: The authors declare no conflict of interest.

References

1. Sanjrani, M.A.; Zhou, B.; Zhao, H.; Bhutto, S.A.; Muneer, A.S.; Xia, S.B. Arsenic contaminated groundwater in China and its treatment options, a review. *Appl. Ecol. Environ. Res.* **2019**, *17*, 1655–1683. [[CrossRef](#)]
2. Raza, M.; Mahjabeen, I.; Fahim, M.; Malik, W.A.; Khan, A.U.; Kayani, M.A.; Akram, Z. Redox balance and DNA fragmentation in arsenic-exposed occupational workers from different industries of Pakistan. *Environ. Sci. Pollut. Res.* **2018**, *25*, 33381–33390. [[CrossRef](#)] [[PubMed](#)]
3. Rathi, B.S.; Kumar, P.S. A review on sources, identification and treatment strategies for the removal of toxic Arsenic from water system. *J. Hazard. Mater.* **2021**, *418*, 126299. [[CrossRef](#)]
4. Dos Santos, H.H.; Demarchi, C.A.; Rodrigues, C.A.; Greneche, J.M.; Nedelko, N.; Ślowska-Waniewska, A. Adsorption of As (III) on chitosan-Fe-crosslinked complex (Ch-Fe). *Chemosphere* **2011**, *82*, 278–283. [[CrossRef](#)]
5. Das, D.; Chatterjee, A.; Samanta, G.; Mandal, B.; Chowdhury, T.R.; Chowdhury, P.; Lodh, D. Arsenic contamination in groundwater in six districts of West Bengal, India: The biggest arsenic calamity in the world. *Analyst* **1994**, *119*, 168N–170N. [[CrossRef](#)]
6. Berg, M.; Tran, H.C.; Nguyen, T.C.; Pham, H.V.; Schertenleib, R.; Giger, W. Arsenic contamination of groundwater and drinking water in Vietnam: A human health threat. *Environ. Sci. Technol.* **2001**, *35*, 2621–2626. [[CrossRef](#)]
7. Hug, S.J.; Leupin, O.X.; Berg, M. Bangladesh and Vietnam: Different groundwater compositions require different approaches to arsenic mitigation. *Environ. Sci. Technol.* **2008**, *42*, 6318–6323. [[CrossRef](#)]
8. Bundschuh, J.; Farias, B.; Martin, R.; Storniolo, A.; Bhattacharya, P.; Cortes, J.; Albouy, R. Groundwater arsenic in the Chaco-Pampean plain, Argentina: Case study from Robles county, Santiago del Estero province. *Appl. Geochem.* **2004**, *19*, 231–243. [[CrossRef](#)]
9. Harvey, C.F.; Ashfaq, K.N.; Yu, W.; Badruzzaman, A.; Ali, M.A.; Oates, P.M.; Islam, S. Groundwater dynamics and arsenic contamination in Bangladesh. *Chem. Geol.* **2006**, *228*, 112–136. [[CrossRef](#)]
10. Smedley, P.L.; Kinniburgh, D.G. A review of the source, behaviour and distribution of arsenic in natural waters. *Appl. Geochem.* **2002**, *17*, 517–568. [[CrossRef](#)]
11. World Health Organization. *The World Health Report 2004: Changing History*; World Health Organization: Geneva, Switzerland, 2004.
12. Ning, R.Y. Arsenic removal by reverse osmosis. *Desalination* **2002**, *143*, 237–241. [[CrossRef](#)]
13. Leupin, O.X.; Hug, S.J. Oxidation and removal of arsenic (III) from aerated groundwater by filtration through sand and zero-valent iron. *Water Res.* **2005**, *39*, 1729–1740. [[CrossRef](#)]
14. Jegadeesan, G.; Mondal, K.; Lalvani, S.B. Arsenate remediation using nanosized modified zerovalent iron particles. *Environ. Prog.* **2005**, *24*, 289–296. [[CrossRef](#)]
15. Kim, T.U.; Drewes, J.E.; Summers, R.S.; Amy, G.L. Solute transport model for trace organic neutral and charged compounds through nanofiltration and reverse osmosis membranes. *Water Res.* **2007**, *41*, 3977–3988. [[CrossRef](#)] [[PubMed](#)]
16. Hansen, H.K.; Núñez, P.; Grandon, R. Electrocoagulation as a remediation tool for wastewaters containing arsenic. *Miner. Eng.* **2006**, *19*, 521–524. [[CrossRef](#)]
17. Owlad, M.; Aroua, M.K.; Daud, W.A.W.; Baroutian, S. Removal of hexavalent chromium-contaminated water and wastewater: A review. *Water Air Soil Pollut.* **2009**, *200*, 59–77. [[CrossRef](#)]
18. Imran, M.; Iqbal, M.M.; Iqbal, J.; Shah, N.S.; Khan, Z.U.H.; Murtaza, B.; Rizwan, M. Synthesis, characterization and application of novel MnO and CuO impregnated biochar composites to sequester arsenic (As) from water: Modeling, thermodynamics and reusability. *J. Hazard. Mater.* **2021**, *401*, 123338. [[CrossRef](#)]
19. Iqbal, M.M.; Imran, M.; Ali, B.; Nawaz, M.; Siddique, M.H.; Al-Kahtani, A.A.; Hussain, K.; Murtaza, B.; Shah, N.S.; Khan, Z.U.H. Nanocomposites of sedimentary material with ZnO and magnetite for the effective sequestration of arsenic from aqueous systems: Reusability, modeling and kinetics. *Environ. Technol. Innov.* **2021**, *21*, 101298. [[CrossRef](#)]
20. Muedi, K.L.; Brink, H.G.; Masindi, V.; Maree, J.P. Effective removal of arsenate from wastewater using aluminium enriched ferric oxide-hydroxide recovered from authentic acid mine drainage. *J. Hazard. Mater.* **2021**, *414*, 125491. [[CrossRef](#)]
21. Rahman, H.L.; Erdem, H.; Sahin, M.; Erdem, M. Iron-incorporated activated carbon synthesis from biomass mixture for enhanced arsenic adsorption. *Water Air Soil Pollut.* **2020**, *231*, 6. [[CrossRef](#)]
22. Hussain, M.; Imran, M.; Abbas, G.; Shahid, M.; Iqbal, M.; Naeem, M.A.; Murtaza, B.; Amjad, M.; Shah, N.S.; Ul Haq Khan, Z. A new biochar from cotton stalks for As (V) removal from aqueous solutions: Its improvement with H₃PO₄ and KOH. *Environ. Geochem. Health* **2020**, *42*, 2519–2534. [[CrossRef](#)] [[PubMed](#)]
23. Nakamoto, K.; Kobayashi, T.J. Arsenate and arsenite adsorbents composed of nano-sized cerium oxide deposited on activated alumina. *Sep. Sci. Technol.* **2019**, *54*, 523–534. [[CrossRef](#)]
24. Tresintsi, S.; Simeonidis, K.; Katsikini, M.; Paloura, E.C.; Bantsis, G.; Mitrakas, M. A novel approach for arsenic adsorbents regeneration using MgO. *J. Hazard. Mater.* **2014**, *265*, 217–225. [[CrossRef](#)] [[PubMed](#)]
25. Salameh, Y.; Albadarin, A.B.; Allen, S.; Walker, G.; Ahmad, M.N.M. Arsenic (III, V) adsorption onto charred dolomite: Charring optimization and batch studies. *Chem. Eng. J.* **2015**, *259*, 663–671. [[CrossRef](#)]
26. Chen, T.; Wei, Y.; Yang, W.; Liu, C. Highly efficient As (III) removal in water using millimeter-sized porous granular MgO-biochar with high adsorption capacity. *J. Hazard. Mater.* **2021**, *416*, 125822. [[CrossRef](#)]

27. Xu, X.; Cao, X.; Zhao, L. Comparison of rice husk-and dairy manure-derived biochars for simultaneously removing heavy metals from aqueous solutions: Role of mineral components in biochars. *Chemosphere* **2013**, *92*, 955–961. [CrossRef]
28. Yao, Y.; Gao, B.; Inyang, M.; Zimmerman, A.R.; Cao, X.; Pullammanappallil, P.; Yang, L. Biochar derived from anaerobically digested sugar beet tailings: Characterization and phosphate removal potential. *Bioresour. Technol.* **2011**, *102*, 6273–6278. [CrossRef]
29. Tauber, M.J.; Mathies, R.A. Structure of the aqueous solvated electron from resonance Raman spectroscopy: Lessons from isotopic mixtures. *J. Am. Chem. Soc.* **2003**, *125*, 1394–1402. [CrossRef]
30. Yadanaparthi, S.K.R.; Graybill, D.; von Wandruszka, R. Adsorbents for the removal of arsenic, cadmium, and lead from contaminated waters. *J. Hazard. Mater.* **2009**, *171*, 1–15. [CrossRef]
31. Deng, Y.; Li, X.; Ni, F.; Liu, Q.; Yang, Y.; Wang, M.; Chen, W. Synthesis of magnesium modified biochar for removing copper, lead and cadmium in single and binary systems from aqueous solutions: Adsorption mechanism. *Water* **2021**, *13*, 599. [CrossRef]
32. Wetteland, C.L.; de Jesus Sanchez, J.; Silken, C.A.; Nguyen, N.-Y.T.; Mahmood, O.; Liu, H. Dissociation of magnesium oxide and magnesium hydroxide nanoparticles in physiologically relevant fluids. *J. Nanoparticle Res.* **2018**, *20*, 215. [CrossRef]
33. Biçer, M.; Şişman, İ. Controlled synthesis of copper nano/microstructures using ascorbic acid in aqueous CTAB solution. *Powder Technol.* **2010**, *198*, 279–284. [CrossRef]
34. Zhu, D.; Chen, Y.; Yang, H.; Wang, S.; Wang, X.; Zhang, S.; Chen, H. Synthesis and characterization of magnesium oxide nanoparticle-containing biochar composites for efficient phosphorus removal from aqueous solution. *Chemosphere* **2020**, *247*, 125847. [CrossRef] [PubMed]
35. Rizwan, M.; Ali, S.; Adrees, M.; Rizvi, H.; Zia-ur-Rehman, M.; Hannan, F.; Ok, Y.S. Cadmium stress in rice: Toxic effects, tolerance mechanisms, and management: A critical review. *Environ. Sci. Pollut. Res.* **2016**, *23*, 17859–17879. [CrossRef] [PubMed]
36. Wang, S.; Gao, B.; Li, Y. Enhanced arsenic removal by biochar modified with nickel (Ni) and manganese (Mn) oxyhydroxides. *J. Ind. Eng. Chem.* **2016**, *37*, 361–365. [CrossRef]
37. Din, S.U.; Mahmood, T.; Naeem, A.; Hamayun, M.; Shah, N.S. Detailed kinetics study of arsenate adsorption by a sequentially precipitated binary oxide of iron and silicon. *Environ. Technol.* **2019**, *40*, 261–269. [CrossRef]
38. Banerjee, K.; Amy, G.L.; Prevost, M.; Nour, S.; Jekel, M.; Gallagher, P.M.; Blumenschein, C.D. Kinetic and thermodynamic aspects of adsorption of arsenic onto granular ferric hydroxide (GFH). *Water Res.* **2008**, *42*, 3371–3378. [CrossRef]
39. Zhu, D.; Yang, H.; Chen, X.; Chen, W.; Cai, N.; Chen, Y.; Chen, H. Temperature-dependent magnesium citrate modified formation of MgO nanoparticles biochar composites with efficient phosphate removal. *Chemosphere* **2021**, *274*, 129904. [CrossRef]
40. Shaheen, S.M.; Niazi, N.K.; Hassan, N.E.; Bibi, I.; Wang, H.; Tsang, D.C.; Rinklebe, J. Wood-based biochar for the removal of potentially toxic elements in water and wastewater: A critical review. *Int. Mater. Rev.* **2019**, *64*, 216–247. [CrossRef]
41. Van Vinh, N.; Zafar, M.; Behera, S.K.; Park, H.S. Arsenic (III) removal from aqueous solution by raw and zinc-loaded pine cone biochar: Equilibrium, kinetics, and thermodynamics studies. *Environ. Sci. Technol.* **2015**, *12*, 1283–1294. [CrossRef]
42. Lin, L.; Zhou, S.; Huang, Q.; Huang, Y.; Qiu, W.; Song, Z. Capacity and mechanism of arsenic adsorption on red soil supplemented with ferromanganese oxide–biochar composites. *Environ. Sci. Pollut. Res.* **2018**, *25*, 20116–20124. [CrossRef] [PubMed]
43. De Almeida Ohana, N.; HM, L.F.; Luis, N.G. Adsorption of arsenic anions in water using modified lignocellulosic adsorbents. *Results Eng.* **2022**, *13*, 100340.
44. Shaikh, W.A.; Alam, M.A.; Alam, M.O.; Chakraborty, S.; Owens, G.; Bhattacharya, T. Enhanced aqueous phase arsenic removal by a biochar based iron nanocomposite. *Environ. Technol. Innov.* **2020**, *19*, 100936. [CrossRef]
45. Cuong, D.V.; Wu, P.C.; Liou, S.Y.H.; Hou, C.H. An integrated active biochar filter and capacitive deionization system for high-performance removal of arsenic from groundwater. *J. Hazard. Mater.* **2022**, *423*, 127084. [CrossRef] [PubMed]
46. Sun, T.; Pei, P.; Sun, Y.; Xu, Y.; Jia, H. Performance and mechanism of As (III/V) removal from aqueous solution by novel positively charged animal-derived biochar. *Sep. Purif. Technol.* **2022**, *290*, 120836. Available online: <https://www.sciencedirect.com/science/article/abs/pii/S1383586622003938> (accessed on 19 September 2022). [CrossRef]
47. Lin, L.; Gao, M.; Song, Z.; Mu, H. Mitigating arsenic accumulation in rice (*Oryza sativa* L.) using Fe-Mn-La-impregnated biochar composites in arsenic-contaminated paddy soil. *Environ. Sci. Pollut. Res.* **2020**, *27*, 41446–41457. [CrossRef]
48. Niazi, N.K.; Bibi, I.; Shahid, M.; Ok, Y.S.; Shaheen, S.M.; Rinklebe, J.; Lüttge, A. Arsenic removal by Japanese oak wood biochar in aqueous solutions and well water: Investigating arsenic fate using integrated spectroscopic and microscopic techniques. *Sci. Total Environ.* **2018**, *621*, 1642–1651. [CrossRef]
49. Lin, M.F.; Nguyen, N.T.; Chen, C.K.; Le, T.T.; Chen, S.S.; Chen, P.H. Preparation of Metal Modified onto Biochar from Hazardous Waste for Arsenic Removal. *J. Nanosci. Nanotechnol.* **2021**, *21*, 3227–3236. [CrossRef]
50. Shen, C.; Gu, L.; Chen, S.; Jiang, Y.; Huang, P.; Li, H.; Xia, D. Sewage sludge derived FeCl₃-activated biochars as efficient adsorbents for the treatment of toxic As (III) and Cr (VI) wastewater. *Environ. Chem. Eng.* **2022**, *10*, 108575. [CrossRef]
51. Balarak, D.; Abasizadeh, H.; Yan, J.-K.; Shim, M.J.; Lee, S.-M. Biosorption of Acid Orange 7 (AO7) dye by canola waste: Equilibrium, kinetic and thermodynamics studies. *Desalin. Water Treat.* **2020**, *190*, 331–339. [CrossRef]
52. Linh, N.L.M.; Van Hoang, D.; Duong, T.; Tinh, M.X.; Quang Khieu, D. Adsorption of arsenate from aqueous solution onto modified Vietnamese bentonite. *Adv. Mater. Sci. Eng.* **2019**, *2019*, 2710926.
53. Sanou, Y.; Samuel, P.J. The Comparative study of adsorption capacity of two mixed materials for arsenic remediation in aqueous solutions. *J. Environ. Treat. Tech.* **2021**, *9*, 559–565.

54. Drweesh, S.A.; Fathy, N.A.; Wahba, M.A.; Hanna, A.A.; Akarish, A.I.; Elzahany, E.A.; Abou-El-Sherbini, K.S. Equilibrium, kinetic and thermodynamic studies of Pb (II) adsorption from aqueous solutions on HCl-treated Egyptian kaolin. *J. Environ. Chem. Eng.* **2016**, *4*, 1674–1684. [[CrossRef](#)]
55. Manzoor, Q.; Nadeem, R.; Iqbal, M.; Saeed, R.; Ansari, T.M. Organic acids pretreatment effect on Rosa bourbonia phyto-biomass for removal of Pb (II) and Cu (II) from aqueous media. *Bioresour. Technol.* **2013**, *132*, 446–452. [[CrossRef](#)] [[PubMed](#)]